Macromolecular Crowding Amplifies Adipogenesis of Human Bone Marrow-Derived Mesenchymal Stem Cells by Enhancing the Pro-Adipogenic Microenvironment

Xiu Min Ang,[1–3,*] Michelle H.C. Lee,[1–3,*] Anna Blocki, PhD,[1–3,†] Clarice Chen, PhD,[1–3] L.L. Sharon Ong, PhD,[4] H. Harry Asada, PhD,[4,5] Allan Sheppard, PhD,[6] and Michael Raghunath, MD, PhD[1,3,7]

The microenvironment plays a vital role in both the maintenance of stem cells in their undifferentiated state (niche) and their differentiation after homing into new locations outside this niche. Contrary to conventional *in-vitro* culture practices, the *in-vivo* stem cell microenvironment is physiologically crowded. We demonstrate here that re-introducing macromolecular crowding (MMC) at biologically relevant fractional volume occupancy during chemically induced adipogenesis substantially enhances the adipogenic differentiation response of human bone marrow-derived mesenchymal stem cells (MSCs). Both early and late adipogenic markers were significantly up-regulated and cells accumulated 25–40% more lipid content under MMC relative to standard induction cocktails. MMC significantly enhanced deposition of extracellular matrix (ECM), notably collagen IV and perlecan, a heparan sulfate proteoglycan. As a novel observation, MMC also increased the presence of matrix metalloproteinase −2 in the deposited ECM, which was concomitant with geometrical ECM remodeling typical of adipogenesis. This suggested a microenvironment that was richer in both matrix components and associated ligands and was conducive to adipocyte maturation. This assumption was confirmed by seeding undifferentiated MSCs on decellularized ECM deposited by adipogenically differentiated MSCs, Adipo-ECM. On Adipo-ECM generated under crowding, MSCs differentiated much faster under a classical differentiation protocol. This was evidenced throughout the induction time course, by a significant up-regulation of both early and late adipogenic markers and a 60% higher lipid content on MMC-generated Adipo-ECM in comparison to standard induction on tissue culture plastic. This suggests that MMC helps build and endow the nascent microenvironment with adipogenic cues. Therefore, MMC initiates a positive feedback loop between cells and their microenvironment as soon as progenitor cells are empowered to build and shape it, and, in turn, are informed by it to respond by attaining a stable differentiated phenotype if so induced. This work sheds new light on the utility of MMC to tune the microenvironment to augment the generation of adipose tissue from differentiating human MSCs.

Introduction

MESENCHYMAL STEM CELLS or multipotent stromal cells (MSCs) are precursor cells in the bone marrow that can differentiate into a variety of mesodermal lineages.[1] Their clinical applications require *ex-vivo* expansion to generate therapeutically relevant cell numbers; however, extended propagation generally results in a loss of self-renewal capacity and multipotentiality.[2] It is increasingly recognized that the *in-vitro* conditions differ greatly from the original tissue microenvironments from which these cells are derived.[3] *In-vivo*, MSCs reside in a physiologically crowded microenvironment that is composed of soluble factors, other cells, and extracellular matrix (ECM) which is crucial in

[1]Department of Biomedical Engineering, National University of Singapore, Singapore, Singapore.
[2]NUS Graduate School for Integrative Sciences and Engineering (NGS), National University of Singapore, Singapore, Singapore.
[3]NUS Tissue Engineering Program, Life Sciences Institute, National University of Singapore, Singapore, Singapore.
[4]Biosystems & Micromechanics Interdisciplinary Research Group (BioSyM), Singapore-MIT Alliance in Research & Technology (SMART), Singapore, Singapore.
[5]Department of Mechanical Engineering, Massachusetts Institute of Technology, Cambridge, Massachusetts.
[6]Liggins Institute, University of Auckland, Auckland, New Zealand.
[7]Department of Biochemistry, Yong Loo Ling School of Medicine, National University of Singapore, Singapore, Singapore.
*These authors share first authorship.
†*Current affiliation:* Singapore Bioimaging Consortium (SBIC), Biomedical Sciences Institute, Singapore, Singapore.

maintaining the self-renewal and preconditioning of progeny daughter cells.[4] Maintenance of phenotype or differentiation is governed by specific cues within each unique local microenvironment.[5] Current strategies aim at mimicking the *in-vivo* conditions by accounting for the cell–cell, cell–ECM, and cell–growth factor interactions via gel systems, surface coatings, and/or nano-texturing of cell culture supports.[6] However, the capacity of MSCs to build their own microenvironments *in-vitro* has long been underutilized. One reason for this is the apparent inefficiency of cultured cells to deposit appreciable amounts of ECM within a useful time window.[7] This is largely due to the highly dilute, aqueous conditions and lack of crowdedness of contemporary cell culture.[8,9] Physiologically, ECM provides macromolecular confinement while the interstitial spaces contain macromolecular solutes. Together, ECM and macromolecular solutes occupy vast parts of a given volume and exclude like-sized molecules through electrostatic repulsion and steric hindrance.[10] However, conventional MSC culture systems containing serum or serum substitutes have a final solute content of 1–10 g/L in culture medium,[10] which is much lower than that observed in interstitial fluids (30–70 g/L)[11,12] or blood plasma (80 g/L).[13]

Macromolecular crowding (MMC) and its effects have been well described in material physics.[10,14] It is defined by exerting an excluded-volume effect (EVE) due to the addition of one or more types of macromolecules into the system. The amount of EVE is dependent on the fraction volume occupancy of the macromolecules.[15] Macromolecular crowders can generate a high level of fractional volume occupancy (FVO), which, in turn, greatly influences equilibria and rates of biochemical reactions that depend on non-covalent associations and/or conformational changes, such as protein and nucleic acid synthesis, intermediary metabolism, cell signaling, gene expression, and fibril formation.[16,17] In an earlier work, we demonstrated that introducing negatively or neutrally charged macromolecules to culture media has strong pleiotropic effects on ECM deposition in various cell types, enabling them to build their respective microenvironments *in-vitro* with greater efficiency and speed.[15,18,19] In this study, we have developed a crowding protocol using a mixture of Ficoll70 (Fc70) and Ficoll400 (Fc400) to create a fraction volume occupancy of ~17% in the culture medium, thereby emulating the crowdedness of the perfused bone marrow compartment.[15] We noted in MSCs not only a markedly increased ECM deposition but also an enhanced adipogenic differentiation when induced under MMC.[15] We hypothesized in this study that this was caused by dynamic cell-matrix reciprocity between MSCs and their *de novo* built microenvironment by which crowding directly affects ECM composition and, thus, indirectly influences cell phenotype.

The worldwide epidemic of obesity and metabolic disease has led to increased interest in adipose tissue and the processes of adipogenesis. Current models of adipogenic cell differentiation and functionality are based on immortalized lines, notably the murine preadipocyte 3T3-L1 cell line.[20] Human stem cells, transdifferentiated or dedifferentiated cells are relatively new models that are attracting increasing interest for the study of adipocyte regulation and physiology due to their greater clinical relevance.[20] The model we describe here encompasses adipogenesis from an uncommitted human mesenchymal precursor cell to a mature phenotype with a much higher degree of maturation than is possible with current protocols.

Materials and Methods

Calculation for emulating bone marrow crowdedness and choice of macromolecular crowder

Since no data are available for the calculation of bone marrow crowdedness, we used blood serum and its dominant component, albumin, as baseline for our calculations for FVO.[15] In brief, the volume occupied by an albumin molecule is calculated to be 268×10^{-27} m,[3] while the number of albumin molecules in 80 mg is 69.8×10^{16}. From these numbers, the FVO occupied by these amount of molecules in 1 mL can be estimated to be $(268 \times 10^{-27}) \times (69.8 \times 10^{16})/10^{-6} = \sim 18\%$ (v/v). To approximate this value with the Ficoll™ (GE Healthcare, Bio-Sciences AB) mixture, we chose concentrations of either crowder adding up to a FVO in our experiments of ~17%.

MSC culture

Human bone-marrow derived MSCs were obtained commercially from Lonza (Lonza/Cambrex Bioscience, PT-2501; Walkersville, Inc.) at passage 2 and cultured in basal culture medium composed of low glucose Dulbecco's-modified Eagle's medium (LGDMEM) supplemented with GlutaMAX™ (10567; Gibco/Life Technologies), 10% fetal bovine serum (FBS) (10270; Gibco/Life Technologies), 100 units/mL penicillin, and 100 μL/mL streptomycin (P/S) (15140; Gibco/Life Technologies). Cells were maintained at 37°C in a humidified atmosphere of 5% CO_2, with medium change twice per week. To prevent spontaneous differentiation, cells were maintained at subconfluent levels before being detached using TrypLE™ Express (12604; Gibco/Life Technologies), passaged at 1:3–4, and cultured to generate subsequent passages. Directed differentiation was carried out with cells at passages 6 to 8.

Adipogenic induction of MSCs

MSCs were seeded at an initial density of 10,500 cm[2] in cell culture well plates. Adipogenic differentiation was stimulated when the cells reached confluence as described (with modifications)[1] via three cycles of 4 days of induction, followed by 3 days of maintenance. Non-induced control MSCs were fed only basal medium on the same schedule. The basal media used in the differentiation process was composed of high glucose Dulbecco's-modified Eagle's medium (HGDMEM) supplemented with GlutaMAX™ (10569; Gibco/Life Technologies), 10% FBS (10270; Gibco/Life Technologies), 100 units/mL penicillin, and 100 μL/mL streptomycin (P/S) (15140; Gibco/Life Technologies) The induction media is supplemented with 0.5 mM 3-isobutyl-1methylxanthine (IBMX) (I5879; Sigma), 0.2 mM indomethacin (I7378; Sigma), 1 μM dexamethasone (D4902; Sigma), and 10 μg/mL insulin (I6634/91077C; Sigma). Basal media alone was used during the maintenance phase. For conditions treated with macromolecular crowding (+MMC), throughout the differentiation process, the media was supplemented with a cocktail of macromolecules; Ficoll™70 (PM70, 17-0310-50; GE Healthcare, Bio-Sciences AB) at 37.5 mg/mL and Ficoll™400 (PM400, 17-0300-50; GE Healthcare, Bio-sciences AB) at 25 mg/mL,

dissolved into media at room temperature with gentle agitation. Media was sterile filtered with a 0.22 μm syringe filter (16532; Satorius Stedim Biotech GmbH) before use.

Deposition and decellularization of matrices by lysis

To generate the lineage-specific matrices–*MSC Matrix*; MSCs were seeded at 3.5×10^4 cells/well in 24-well plates (662160; Cellstar, Greiner; Bio-one GmbH) and maintained in basal media ± crowder for 7 days before lysis. *Adipocyte matrix*; MSCs in T175 flasks (431080; Corning) were adipogenically induced for 2 weeks before being seeded at a density of 3.5×10^4 cells/well in 24-well plates (662160; Cellstar, Greiner, Bio-one GmbH) and treated to 1 cycle of adipogenic induction/maintenance ± crowder for 7 days before lysis. For lysis, monolayers were first washed with Phosphate-Buffered Saline (PBS) (BUF-2040, 1st Base, Singapore) twice and then treated with 0.5% Sodium Deoxycholate (DOC) (2003030085; Prodotti Chimici E Alimentari S.p.A.) supplemented with 0.5× Complete Protease Inhibitor (11836145001; Roche Diagnostics GmbH) in water four times for 15 min each at room temperature, followed by 0.5% DOC in PBS for 30 min at RT on a nutating platform. Matrices were then incubated with DNAse (D3200-01; US Biologicals) for 1 h at 37°C, and then washed thrice with PBS.

Nile Red adherent cytometry to assess area of cytoplasmic lipid accumulation

After 21 days (corresponding to three complete induction cycles), cell cultures were rinsed with PBS, fixed in 4% methanol-free formaldehyde (28908; Pierce Biotechnology, Inc.) for 30 min at RT, and then co-stained for 30 min with 5 μg/mL Nile Red (N3013; Sigma), for cytoplasmic lipid droplets and 0.5 μg/mL of 4′,6-diamidino-2-phenylindole (DAPI) (D3571, Molecular Probes®; Life Techonologies) for nuclear DNA as previously described.[21] Adherent cytometry was performed according to previously described protocol.[18] Nine image sites per well were acquired using 2× magnification with a cool-SNAP HQ camera attached to a Nikon TE2000 microscope (Nikon Instruments), stored, and analyzed using the Metamorph Imaging System Software 6.3v3 (Molecular Devices). An image field of 4.48×3.34 mm per site was defined for each 24-well plate with a final image of 13.43×10.03 mm; covering 134.70 mm² per well. Nile Red was viewed under a rhodamine filter [Ex572 nm/Em630 nm], while DAPI fluorescence was assessed with a DAPI filter [Ex350 nm/Em465 nm]. The Cell Count module was used for cell enumeration, while the Integrated Morphometry Analysis module was used to evaluate the area of fluorescent Nile Red staining. A specified threshold defined by fluorescent intensity below a defined pixel value was subtracted to eliminate background area. In addition, triangle masks were applied to remove autofluorescence of corners. Extent of adipogenic differentiation was quantified by area of Nile Red fluorescence from thresholded events normalized to nuclei count. End data corresponded to total area of lipid droplets present per well normalized to cell number (μm²/nuclei), and the average of biological triplicates was taken.

Flow-activated cytometry to assess percentage of cells that have differentiated

Cells were seeded in a six-well plate format (657160; Cellstar, Greiner, Bio-One GmbH). Monolayers were washed twice in PBS, trypsinised, and pelleted by centrifugation for 5 min at 200 g. ~100k cells per sample were fixed with 1% methanol-free formaldehyde (28908; Pierce Biotechnology, Inc.) for at least an hour at 4°C, then stained with Nile Red (10 μg/mL in PBS) for 30 min in the dark at room temperature.[22] Samples were washed and resuspended in PBS, filtered (to remove debris), and acquired using a Beckman Coulter CyAn™ ADP Analyzer (Beckman Coulter, Inc.). Nile Red fluorescence was measured on the FL2 emission channel through a 585±21 nm band pass filter, after excitation with an argon ion laser source at 488 nm. Using a forward scatter (FSC)/side scatter (SSC) representation of events, a gating region was defined to exclude cellular debris from the analysis. Using an overlay histogram (event count/FL2) with non-induced MSCs stained with Nile Red as background control, a bar region was established on the gated population to count cells with high FL2 values (adipocytes). Data analysis was performed using Summit 4.3 software (Beckman Coulter, Inc.). Each sample represents 5000 gated events. Results were expressed as a percentage of cells appearing in the bar region.

Gene expression analysis

Total RNA was extracted from monolayers in a 12-well plate format using the Trizol (15596; Gibco/Life Technologies) chloroform (C2432; Sigma) method followed by the RNeasy® Mini Kit 250 (74106; Qiagen) following the manufacturer's protocol. cDNA were synthesized from isolated mRNA using the Maxima™ First-strand cDNA synthesis kit (K1642; Fermentas, Thermo Fisher Scientific, Inc.). Real-time quantitative polymerase chain reactions (RT-PCR) were performed and monitored on a real-time PCR instrument (MxPro 3000P QPCR; Stratagene, Integrated Sciences) using Maxima™ SYBR Green/ROX qPCR Master Mix (K0222; Fermentas, Thermo Fisher Scientific, Inc.). Data analysis was carried out with the MxPro software v4.01 (Stratagene, Integrated Sciences). For each cDNA sample, the Ct value was defined as the cycle number at which the fluorescence intensity reached the amplification based-threshold fixed by the instrument software. Relative gene expression levels were determined using the $\Delta\Delta^{-Ct}$ method with human ribosomal phosphoprotein P0 (RPLP0) levels serving as an endogenous control. Primer sequences used are shown in Supplementary Table S1 (Supplementary Data are available online at www.liebertpub.com/tea).

Immunocytochemistry of ECM deposition

Monolayers were fixed with 4% methanol-free formaldehyde (28908; Pierce Biotechnology, Inc.) for 10 min at RT or 100% methanol (M/4058/17; Fisher Scientific) for 10 min at −20°C, then blocked with 3% bovine serum albumin (BSA) (Fluka-05488; Sigma) in PBS for an hour. Immunofluorescence was carried out using primary antibodies mouse anti-human collagen I 1:1000 (C2456; Sigma); rabbit anti-human fibronectin 1:100 (A0245; Dako); rabbit anti-human collagen IV 1:500 (6586; Abcam); mouse anti-human heparan sulfate proteoglycan 2 [A76] 1:100 (26265; Abcam) and incubated for 16 h at 4°C. The secondary antibody used was AlexaFluor® 488 chicken anti-rabbit (A21441; Molecular Probes, Life Techonologies) at 1:400 dilution, and Alexa-Fluor® 488 goat anti-mouse (A11029; Molecular Probes, Life Technologies) at 1:400 dilution incubation of 1 h at room

temperature. For visualization of the cellular components, samples were incubated with AlexaFluor 488 phalloidin (A12379; Molecular Probes, Life Techonologies) at 1:40 and SelectFX® AlexaFluor 488 Endoplasmic reticulum labeling kit (S34200; Molecular Probes, Life Techonologies) at 1:1000 for 10 min. Cell nuclei were counterstained with 0.5 μg/mL 4′,6-diamidino-2-phenylindole (D1306; Molecular Probes, Life Technologies). Images were captured with an IX71 inverted fluorescence microscope (Olympus). Adherent cytometry was performed according to previously described protocol.[18] Nine image sites per well were acquired using 2× magnification with a coolSNAP HQ camera attached to a Nikon TE2000 microscope (Nikon Instruments), stored, and analyzed using the Metamorph Imaging System Software 6.3v3 (Molecular Devices, Sunnyvale). An image field of 4.48×3.34 mm per site was defined for each 24-well plate with a final image of 13.43×10.03 mm, covering 134.70 mm^2 per well. Fluorescent ECM proteins were viewed under an FITC filter [Ex492 nm/Em535 nm], while DAPI fluorescence was assessed with a DAPI filter [Ex350 nm/Em465 nm]. The Cell Count module was used for cell enumeration, while the Integrated Morphometry Analysis module was used to evaluate the area of fluorescent FITC staining. A specified threshold defined by fluorescent intensity below a defined pixel value is subtracted to eliminate background area. In addition, triangle masks were applied to remove autofluorescence of corners. Extent of ECM deposition was quantified by the area of FITC fluorescence from thresholded events normalized to nuclei count. End data corresponded to total area of ECM deposition present per well normalized to cell number (μm^2/ nuclei). The end data per well are substracted from its corresponding secondary antibody conjugate control before the average of biological triplicate is taken.

Western blotting of harvested media samples

Media were harvested from MSCs 4 days post adipogenic induction (±MMC), mixed with 1×Laemmli buffer containing β-mercaptoethanol (M6250; Sigma). Samples were resolved using the NuPAGE tris-acetate 3–8% gradient pre-cast gel system (EA0375BOX; Gibco/Life Technologies) and transferred to a 0.45 μm nitrocellulose membrane (162-0115; Bio-Rad) according to the manufacturer's protocol. Membranes were blocked with 5% non-fat milk (170-6404; Bio-Rad) in TBST pH 8 (20 mMTris-base–150 mMNaCl–0.05%Tween-20) for 1 h at RT. Subsequently, the primary antibody mouse anti-human Procollagen Type I C-Peptide (42024; QED Bioscience, Inc.) was incubated at a 1:200 dilution with 1% nonfat milk in TBST and was incubated for 1 h at RT. Bound primary antibody was detected with goat anti-mouse HRP (P0447; Dako) diluted 1:1000 in 1% nonfat milk in TBST for 1 h at RT. The membrane was then incubated with Amersham ECL Plus Western Blotting detection reagent (RPN2132; GE Healthcare UK Ltd.), and chemiluminescence was captured with a VersaDoc Imaging System Model 5000 (Bio-Rad).

Analysis of the extent of reticular matrix formation

Automated image processing methods were developed to quantify the directional ECM alignment as represented by Col IV immunostaining and the number of "spaces" within the matrix. We define spaces as regions confined by, and devoid of, ECM. The image processing was carried out using

algorithms in MATLAB (Mathworks) via custom scripts as illustrated in the Supplementary data; see Image Processing Workflow Diagram. To obtain the directional coherence of the Col IV structure, we transformed the image to a different domain using the Hough transform. The domain reduces the image to a set of independent directional distributions with regard to the x-axis. We displayed the directional coherence in a graphical representation with an angle histogram (rose plot). The directional distributions from the Hough transforms are sorted into 40 equally spaced bins of angles between 0 and 360 degrees. The number of elements corresponding to each interval is represented by a petal of the rose, plotted with its apex at the origin. To calculate the number of spaces in the Col IV meshwork, from a binary image obtained via intensity thresholding, we traced the boundaries of the holes inside all connected components (objects). To exclude artifacts, we then removed traced holes with an average diameter fewer than 26 μm or exceeding 300 μm.

Zymography and matrix metalloproteinases assays

The cell layers at various time points and conditions were lysed directly in 1×Laemmli buffer for each sample with mechanical scraping, and the cell lysates were transferred into tubes and stored at −80°C. Cell media was also harvested and stored at −80°C. Gelatin zymography was performed using adapted protocol.[23] Gel was incubated in zymography washing buffer (2.5% Triton X-100, 50 mM Tris.Cl, 5 mM CaCl$_2$, 1 μM ZnCl$_2$, and pH 7.4) for an hour at RT and washed once for 10 min with water. Subsequently, gel was incubated for 16 h at 37°C in zymography reaction buffer (50 mM Tris.Cl, 5 mM CaCl$_2$, 1 μM ZnCl$_2$, and pH 7.4). After PageBlue (24620; Thermo Fisher Scientific, Inc.), staining gel was viewed using the GS-800 Calibrated Densitometer (Bio-Rad), and analyzed using the Quantity One Imaging software v4.5.2 (Bio-Rad). The protease activity assay for bacterial collagenase was performed according to the manufacturer's protocol (E12055; EnzChek, Molecular Probes; Life Techonologies) in a concentration of 0.01 U/mL in standard reaction buffer (control) or in the presence of macromolecules (+MMC). Fluorescent intensity was measured every 10 min for more than 2 h with a microplate reader (PHERAstar, BMG Labtech). Functions of fluorescent gain were estimated by linear regression with the slope of the function indicating the degradation speed of the protease.

Statistical analysis

Unless otherwise stated, all assays were performed in triplicate, and results were reported as means±standard deviation. For Figure 7, and Supplementary Figure 6, one-way ANOVA statistical analysis was performed ($p < 0.001$) followed by Tukey–Kramer Multiple-Comparisons Test. All other statistical analysis was performed using Student's t-test. $*p < 0.05$, $**p < 0.01$, and $***p < 0.001$.

Results

MMC enhances adipogenesis

Chemically induced adipogenesis of MSCs after an induction period of 21 days resulted in MSCs acquiring a more rounded morphology as they differentiated into adipocytes. MSCs are deemed to attain a mature adipocyte phenotype

when there is a significant accumulation of cytoplasmic lipid droplets.[24] Nile Red staining, normalized to cell count, (Fig. 1A) revealed considerably greater accumulation of lipid droplets of MSCs differentiating into adipocytes under induction with MMC conditions as compared with chemical induction alone. This pronounced increase was seen throughout the 21 day time course of induction with a 24% increase on day 21 as opposed to non-MMC controls. Since staining was normalized to cell numbers, it further indicated that each differentiated cell contained more lipid droplets under MMC compared with non-MMC controls. However, there was no difference in the proportion of MSCs that differentiated into adipocytes with (58.9% ± 0.2%) or without (69.7% ± 4.4%) MMC (Fig. 1B). Cell layers that were maintained in basal media in the presence or absence of MMC did not express lipid droplets at any time point, confirming that the MMC composition *per se* was not inherently adipogenic (Supplementary Fig. S1). In addition, gene expression analysis confirmed, throughout the time course of induction, a higher level of induction of early (PPAR-γ), mid (GLUT4 and FABP4) and late (leptin) adipogenic genes under MMC-amplified adipogenesis (Fig. 2). Taken together, the data show that MMC enhances adipogenesis in differentiating MSCs.

MMC increases matrix deposition

MMC was previously shown to increase matrix deposition in various cell types.[15] In this study, the addition of MMC to adipogenically differentiating MSCs increased the matrix deposition of collagen IV (Col IV), heparan sulfate proteoglycans (HSPG), and fibronectin (FN) significantly compared with conventional induction alone (Fig. 3), and this was evident from day 14 onward. At the end of day 21, the amounts of both Col IV and HSPG were quadrupled in comparison to non-MMC controls (Fig. 3A, B). Interestingly, there was a decrease in FN from day 14 to day 21 (Fig. 3C) only in the MMC cultures with the final amount being 43% lower than conventional induction alone. This correlates with the stoichiometric changes in ECM composition described for the differentiation of murine preadipocytes—the reduction of the bone marrow-typical matrix components collagen I (Col I) and fibronectin (FN) and the increased presence of collagen IV (Col IV).[24–27] To further assess the changes in ECM composition that occur during adipogenic differentiation, amount and distribution of ECM components normalized to cell number were compared between undifferentiated MSCs and differentiated adipocytes after 3 weeks of induction with
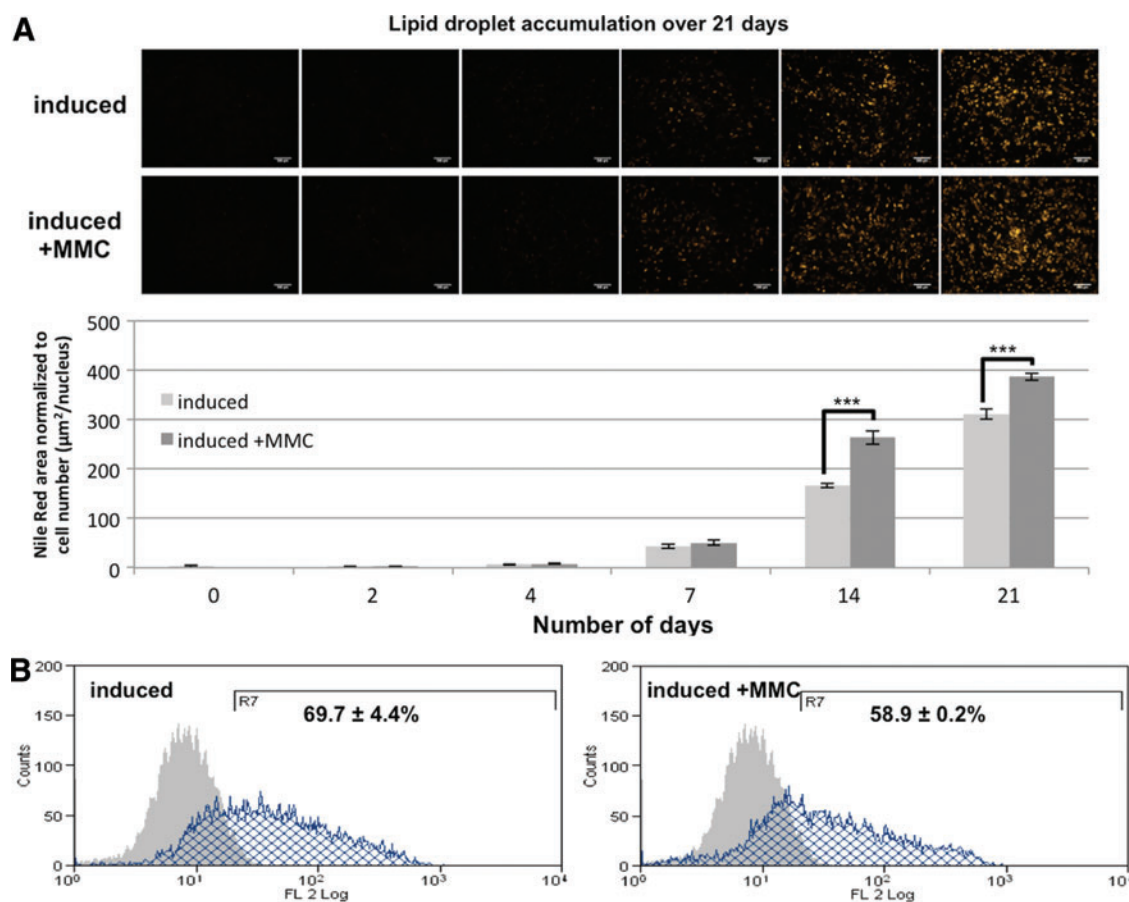

FIG. 1. Macromolecular crowding (MMC) increases the accumulation of lipid droplets of mesenchymal stem cells (MSCs) during adipogenic differentiation for 21 days. **(A)** Quantitative analysis of the fluorescence area normalized to cell number showed significantly more lipid storage when MSCs are adipogenically induced +MMC. Scale bar: 500 μm. **(B)** Flow cytometry gating shows no significant difference between percentage of lipid droplet–laden cells in conventionally induced (69.7% ± 4.4%) and induced +MMC (58.9% ± 0.2%) MSCs. This run was performed in duplicate. Student's *t*-test *$p < 0.05$, **$p < 0.01$ and ***$p < 0.001$. Color images available online at www.liebertpub.com/tea
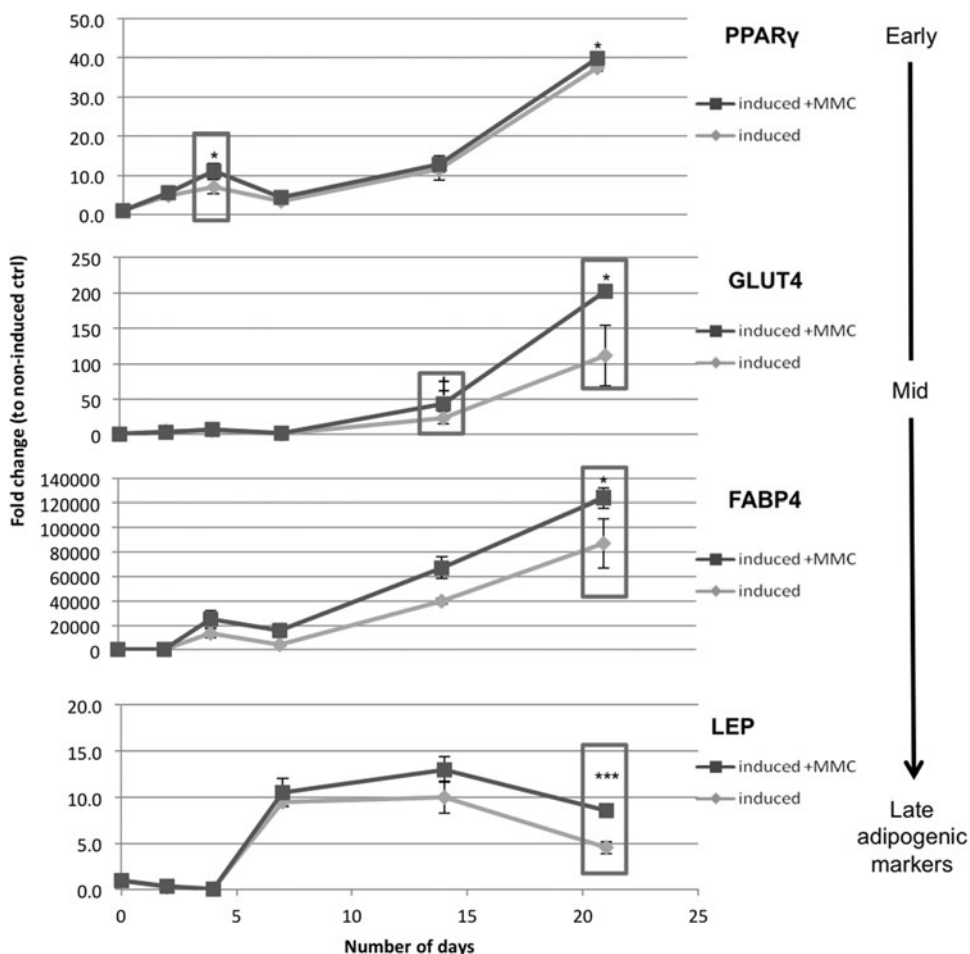
FIG. 2. MMC up-regulates the expression of early to late adipogenic genes of MSCs undergoing adipogenesis for 21 days. mRNA analyses demonstrated commitment of MSCs to adipogenic lineage, with induced +MMC expressing differentially up-regulated gene response throughout the entire differentiation period. In particular, PPARγ, the master regulator of adipogenic differentiation, shows an increased expression under induced +MMC condition as early as day 4. Late adipogenic genes GLUT4, FABP4, and LEP followed with significant up-regulation under induced +MMC conditions at day 21. PPARγ, peroxisome proliferator-activated receptor gamma; GLUT4, glucose transporter type 4; FABP4, fatty acid binding protein 4; LEP, leptin. ‡Borderline significance at $p = 0.05$. $*p < 0.05$, $**p < 0.01$ and $***p < 0.001$.

and without MMC (Fig. 4). As expected, Col IV deposition was higher in differentiated cultures compared with their undifferentiated controls (Fig. 4A). On the other hand, while HSPG deposition decreased under non-MMC induction cultures (−MMC group in Fig. 4B), HSPG deposition increased approximately two-fold compared with undifferentiated controls under MMC condition (+MMC group in Fig. 4B). Moreover, while there was an increased deposition of FN in differentiated adipocytes compared with non-induced MSCs cultured in the absence of MMC [Fig. 4D (−MMC group)], MMC cultures, in contrast, showed declining Col I and FN content of the ECM when similarly induced for adipogenic differentiation [Fig. 4C, D (+MMC group)]. These results correspond with previous findings in a murine cell culture system of a reduction of Col I and FN when adipogenesis takes place.[25] However, a comparison of Col I could not be performed accurately on non-crowded cultures, as there was minimal deposition of Col I (top panel figures in Fig. 4C), compared with the same cultures performed in MMC conditions (bottom panel figures in Fig. 4C), due to the effect of enhanced proteolytic processing of procollagen I to collagen I (see next section). Distinct remodeling of the ECM occurred during the differentiation process. The more parallelly aligned deposition pattern of Col IV was transformed to a more honeycomb-like structure (Fig. 4A). This remodeling pattern was also evident for HSPG (Fig. 4B), Col I (Fig. 4C) and FN (Fig. 4D). Across the four ECM proteins, the morphological change in structure in the course

of adipogenesis was most pronounced under MMC (Fig. 4 [10×], and Supplementary Fig. S2 [20×]).

MMC enhances the proteolytic processing of procollagen I to collagen

The negatively charged crowder dextran sulfate enhances collagen deposition via enhanced proteolytic processing of Col I by BMP-1 in fibroblasts.[8,9] We ascertained by immunoblotting for the C3 Col I propeptide trimer that the same mechanism was operational under mixed neutral crowding with MSCs (Supplementary Fig. S3) and confirmed an increase in cleaved C-propeptide for media samples with MMC (Supplementary Fig. S3A, red arrow), accompanied by a corresponding decrease in procollagen bands. Densitometry quantified a 25.5-fold increase in C3 fragment in cultures under MMC (Supplementary Fig. S3B), confirming enhanced proteolytic processing of Col I by differentiating MSCs under MMC. This is evident where Col I deposition is enhanced under MMC conditions regardless of adipogenic induction (Fig. 4) compared with the minimal Col I deposition for corresponding non-crowded controls.

MMC increases matrix remodeling via accelerated metalloproteinase activity

Besides an accelerated BMP-1 activity, MMC also increased the activity of matrix metalloproteinases (MMPs) associated
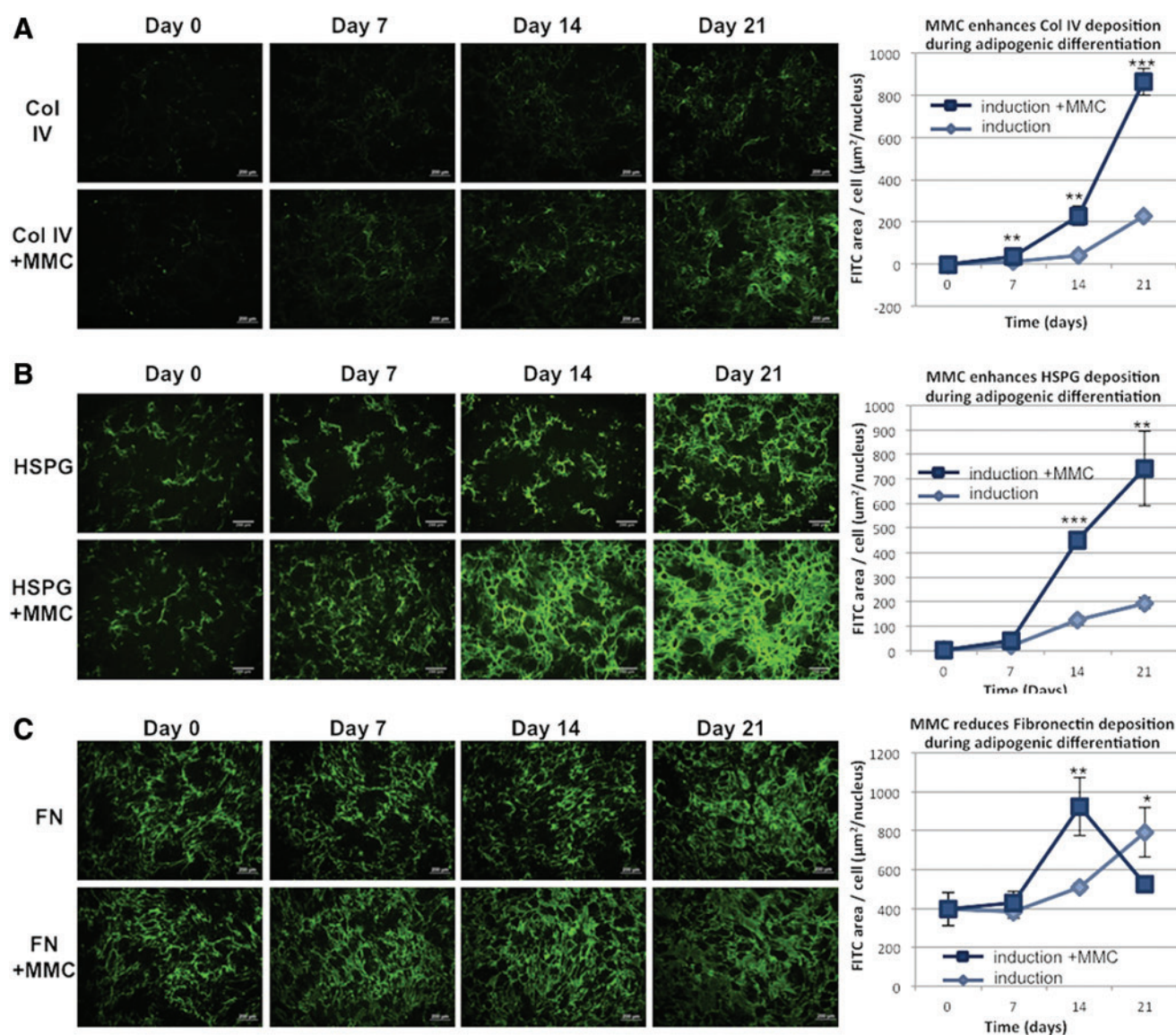
FIG. 3. MMC induces pronounced changes of various extracellular matrix (ECM) components en route to an adipogenic matrix during 21 days of adipogenic differentiation of MSCs. Representative immunocytochemistry images throughout the 21-day period showed an increase in deposition of **(A)** Col IV and **(B)** heparin sulfate proteoglycan (HSPG), with this increase visibly more enhanced in induced +MMC conditions. On the other hand, **(C)** under induced +MMC condition, reduction in fibronectin (FN) deposition was observed on d21, which correlated with the literature demonstrating FN reduction during adipogenesis.[25] Corresponding quantitative analyses show fluorescence area normalized to cell number. Scale bar: 200 μm. *$p < 0.05$, **$p < 0.01$ and ***$p < 0.001$. Color images available online at www.liebertpub.com/tea

with the transforming ECM during adipogenesis. Gelatin zymography performed on cell layers of MSCs undergoing adipogenic differentiation showed the presence of a ∼60–65 kDa band, corresponding to MMP-2 (62 kDa active form), which is present in MSCs undergoing adipogenic differentiation[27,28] (type IV collagenase, gelatinase A). In zymography, MMPs digest gelatin within the SDS-PAGE gel under the same conditions. Therefore, the thickness of the bands corresponds to the amount of MMPs present within the sample. The amount of MMP-2 gradually decreased during the course of adipogenic differentiation (Fig. 5A, B), but at each time point, MMC-induced samples contained higher amounts of MMP-2 in the cell layer as compared with standard conditions, with a significant 29% increase at day 7 (Fig. 5B). Interestingly, amounts

of MMP-2 did not change in the culture medium (Supplementary Fig. S4), indicating that under MMC more MMP-2 is incorporated into the ECM. Using a standard protocol, which allows plotting a linear function of gelatin digestion by collagenase type IV (Clostridium histolyticum), the digestion rate (slope or gradient) was estimated by linear regression. In the presence of MMC, the digestion velocity of the collagenase type IV was increased by 22%, indicating that MMC has an enhancing effect on a collagenase type IV activity (Fig. 5C).

MMC enhances the formation of reticular matrix during adipogenesis

To quantify the remodeling of Col IV geometry observed under MMC-augmented adipogenesis, automated image
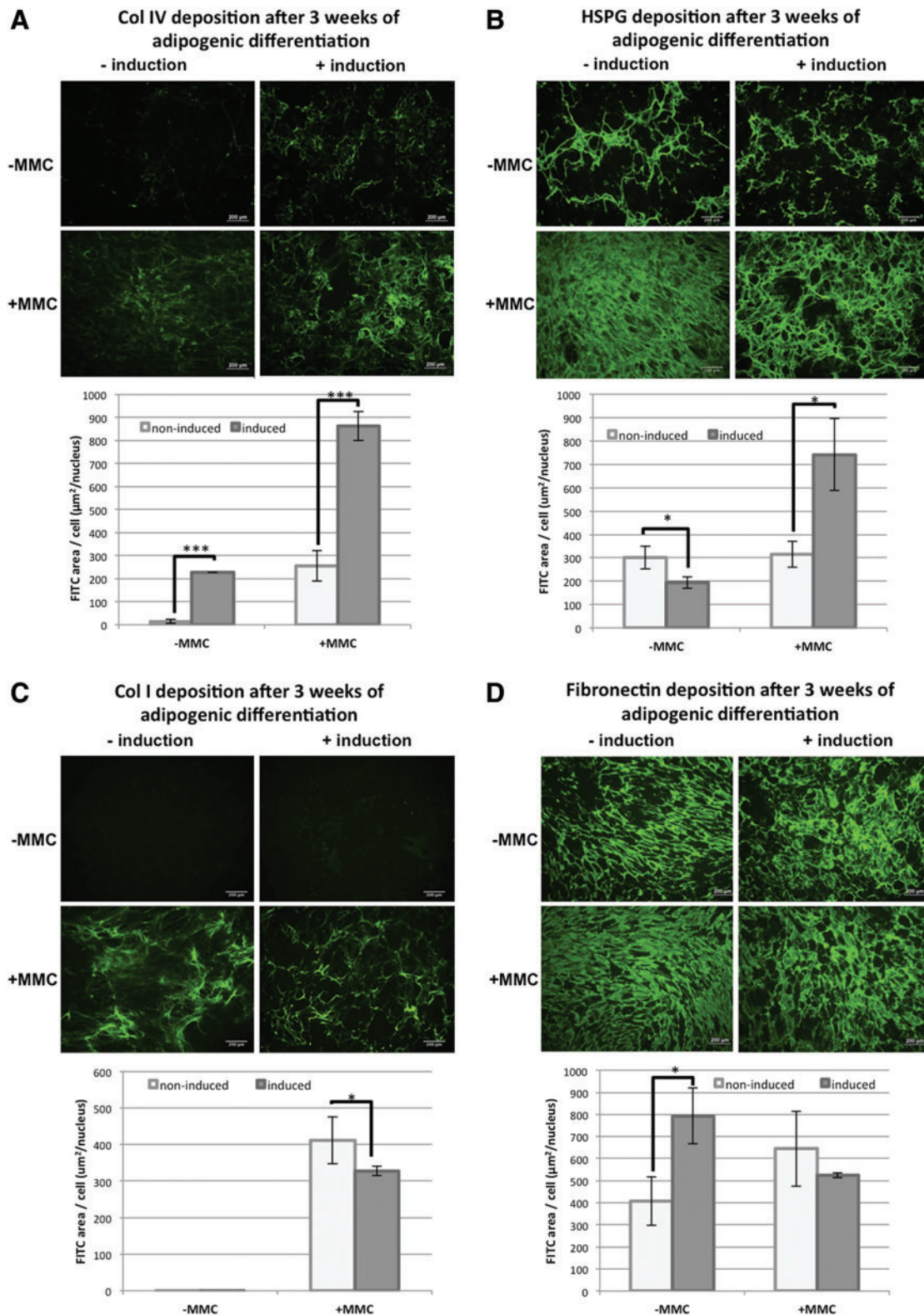
FIG. 4. Enhanced state of deposition and remodeling of adipogenic ECM under MMC after 21 days of adipogenic differentiation. Representative immunocytochemistry images of **(A)** Col IV, **(B)** HSPG, **(C)** Col I, and **(D)** FN of MSCs that underwent adipogenic differentiation±MMC compared to nondifferentiated (-induction) controls. Induced +MMC conditions showed the stoichiometric increase in Col IV and HSPG with the concomitant decrease of Col I and FN compared with its noninduced controls [gray bars vs. white bars of (+MMC group)]. The dynamic remodeling of the various matrix proteins from a fibrillar to a recticular conformation as a result of adipogenic differentiation (left images to right images) was more evident under +MMC conditions (bottom panel). Corresponding quantitative analyses show fluorescence area normalized to cell number. Scale bar: 200 μm. *$p < 0.05$, **$p < 0.01$ and ***$p < 0.001$. Color images available online at www.liebertpub.com/tea
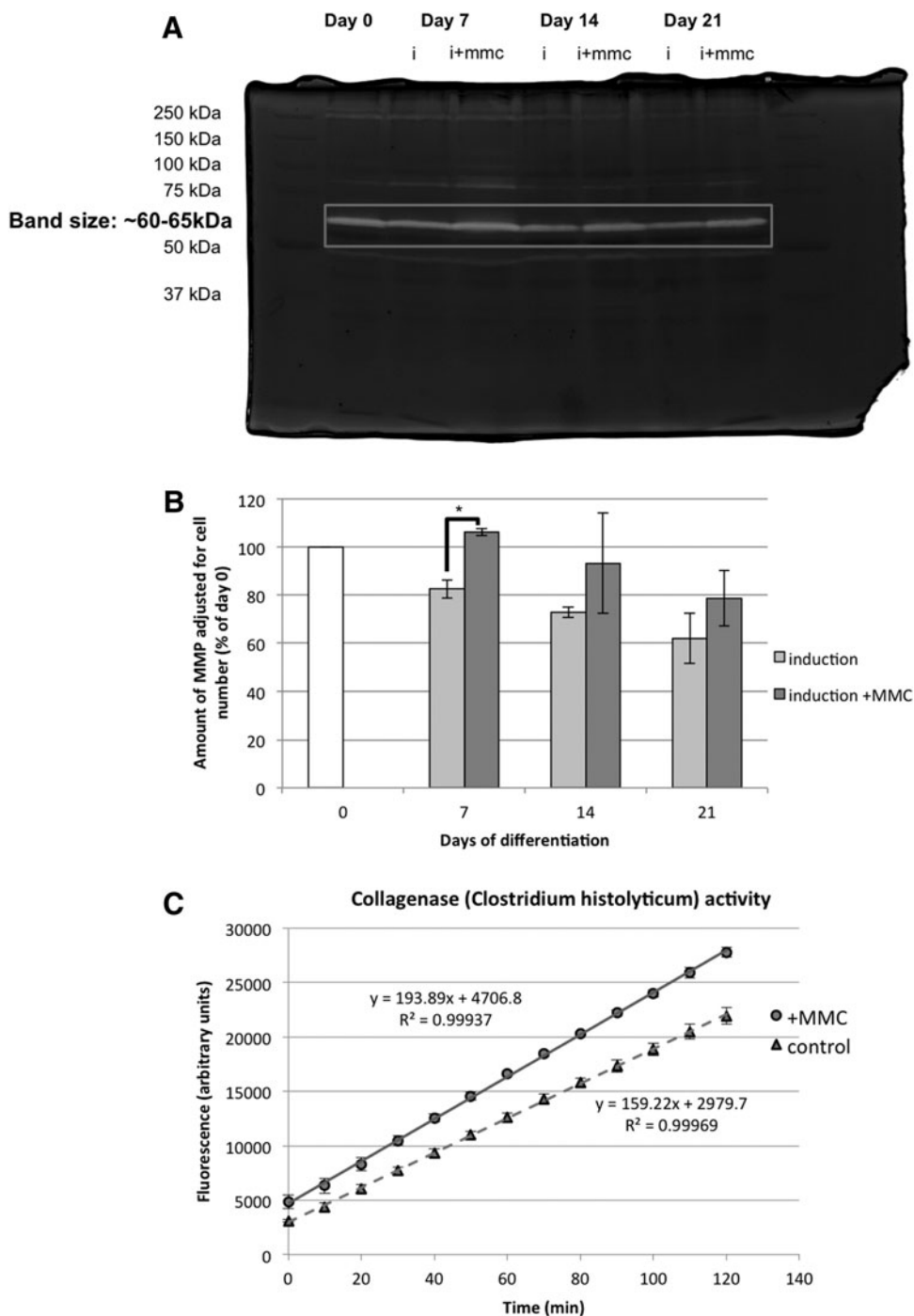
FIG. 5. Enhanced presence of MMP-2 in cell layer of adipogenically induced MSCs and enhanced collagenase activity in the presence of MMC. **(A)** Gelatin zymography of MSCs undergoing adipogenic induction at various time points to assess amount of MMP evident as white bands of size ∼60–65 kDa. At day 7, MMC-induced samples had a significant 29% increase in the amount of MMP in comparison to conventionally induced cells. **(B)** Amount of MMP as a percentage of day 0 quantified by densitometric quantitation of zymographic bands adjusted for cell number. **(C)** Enzyme activity assay of bacterial collagenase type IV. In the presence of MMC, digestion velocity is increased by 22%. $*p < 0.05$.

processing methods using MATLAB were employed to analyze the Col IV-stained images from Figures 3 and 4. Two parameters were assessed: directional alignment and the number of spaces in the ECM. Rose plots (angle histograms) were used to describe the extent of directional alignment. Col IV deposited by naïve MSCs exhibited a small range of angles with small amplitudes of each angle (two-fold at 90°), depicting an aligned matrix [Fig. 6A (i)]. However, this alignment pattern of naïve MSCs was amplified under MMC (five-fold at 90°) [Fig. 6A (ii)]. Under adipogenic induction, but without MMC, the rose plots exhibited a "fan-shaped"

pattern, indicative of a greater range of both angles and amplitude (20-fold at 90°) [Fig. 6A (iii)]. The "fan-shaped" pattern was even more pronounced when the cells were differentiated under MMC (>20-fold at 90°) [Fig. 6A (iv)]. This suggests a more defined reticular network of Col IV representative of an adipogenic matrix.[25] To investigate the temporal dynamics of this remodeling, we compared rose plots at different time points and found that under conditions of induction with MMC, remodeling was more evident from day 7 onward (Fig. 6B), paralleling the dynamics of deposition seen earlier (see Fig. 3A).

The number and size of spaces in the Col IV matrix were also assessed. Not surprisingly, there were very few spaces in the Col IV matrices deposited by naïve MSCs with or without MMC (Fig. 6C (i), white bars). In contrast, adipogenically induced cells had a larger number of spaces without crowding, which was even further increased with MMC, (Fig. 6C (i), grey bars). Further, the diameter of the spaces was greater under induction, irrespective of MMC (data not shown). As with directional alignment (see Fig. 6B), the increase in the number of spaces was significant from day 7 onward [Fig. 6C (ii)].

MMC-generated matrices drives adipogenesis to a greater extent

We hypothesized that MMC enhances the creation of a pro-adipogenic microenvironment by MSCs undergoing adipogenic differentiation that supports greater and faster lipid accumulation. To this end, we seeded undifferentiated MSCs onto decellularized matrices that had been laid down by undifferentiated MSCs (MSC-ECM±MMC) and differentiating MSCs (Adipo-ECM±MMC) and subjected them to the standard chemical induction of 21 days, with MSCs seeded on TCPS as the standard control. The decellularization process was effective in removing the cellular content while retaining the matrix components (Supplementary Fig. S5). Differentiation capacities of these cells were then evaluated based on the abundance of lipid accumulated. Naïve MSCs re-seeded on Adipo-ECM (+MMC) matrices and subjected to standard chemical induction accumulated visibly more droplets (Fig. 7A), which corresponded to a 60% increase of fluorescent Nile Red area compared with TCPS+ind standard control (Fig. 7B). In addition, relative mRNA expression levels for PPARγ in MSCs chemically induced on the Adipo-ECM (+MMC) matrices were ~30% higher than those differentiated on TCPS+ind standard control (Fig. 7C). In addition to this, we observed that MSCs re-seeded and differentiated on decellularized MSC-ECM (±MMC) accumulated ~50% less lipid droplets compared with MSCs differentiated on TCPS+ind control and achieved only ~25–40% of lipid droplet accumulation compared with those re-seeded on the Adipo-ECM (±MMC) (Fig. 7B), suggesting a dampening effect on adipogenesis of this matrix.

To assess the effect of this enhanced pro-adipogenic microenvironment on the speed of differentiation, we performed the same experiment but examined the lipid droplet accumulation already after 10 days of standard chemical induction (instead of the full 21 days). At this time point, MSCs grown on TCPS only showed very low levels of Nile Red-positive areas. In contrast, MSCs grown on Adipo-ECM and Adipo-ECM (+MMC) showed accelerated adipogenesis, with lipid droplets clearly visible at day 10. Nile Red-positive area against TCPS control increased by a factor of 34 (Adipo-ECM) and a statistically significant further increase of five-fold (Adipo-ECM+MMC) when compared with Adipo-ECM alone without MMC (Supplementary Fig. S6).

Naïve MSCs that were re-seeded onto various matrices without chemical induction did not exhibit significant lipid droplet accumulation after 21 days, except for those which were placed on Adipo-ECM (+MMC) matrices. Here, we observed a five-fold increase in Nile red fluorescence area, even though this amount is five-fold less than the TCPS induction control, suggesting spontaneous adipogenic differentiation (Fig. 7D).

Discussion

MMC is a well-researched phenomenon in physical chemistry and biophysics and studied in the realm of protein folding[29] and nucleic acid hybridization.[30] Although such crowding is a ubiquitous feature of cellular systems, MMC is surprisingly understudied and underutilized in biological systems.[10] We have successfully generated a degree of crowdedness for MSCs in-vitro that is modeled after their physiological microenvironment in the bone marrow.[15] Using currently published ranges of biologically active fraction volume occupancies (FVO) that are created by macromolecular crowders,[31] we optimized a mixture of neutrally charged Ficoll 70 and 400 to generate a FVO of ~17%. Other considerations were that these macromolecules do not increase viscosity of culture media,[32] which would be crucial for bioreactor-based work, and that these crowders are already in use for clinical preparations of mononuclear cell fractions of peripheral blood.[33] Due to a lack of published information on the detailed biophysical parameters of the bone marrow, we based our calculations for FVO generation on serum albumin as a principal component of plasma macromolecules. The novel culture composition greatly facilitated MSCs to build and remodel its surrounding microenvironments. Specific ECM components and their composition play a key role in both onset and maintenance of adipogenic differentiation.[34] In particular, Col IV, the major component of basement membranes, provides structural support for mature lipid-laden adipocytes. It has been shown to be synthesized by MSCs and to affect their adipogenic differentiation.[27] Accordingly, we

FIG. 6. Collagen IV is remodeled extensively from a fibrillar to a reticular honeycomb structure in adipogenically induced MSCs under MMC. **(A)** Rose plots of Col IV directional alignment after 21 days of adipogenic differentiation. Inserts show corresponding Col IV images. (i) & (ii) For non-induced conditions, rose plots exhibited a smaller range of angles with smaller amplitudes, corresponding to a more fibrillar network. When adipogenically induced (iii), a shift toward a fan-shaped pattern indicated a transition to a reticular network, (iv) but was more pronounced under +MMC with a larger amplitude. **(B)** Similarly, rose plots during the course of adipogenic differentiation reveal that (i) both range of angles and amplitude increased over time, and (ii) the onset of remodeling occurred earlier (day 7) for the induced +MMC condition. **(C)** (i) Space analysis of Col IV at day 21 reveals an increased number of spaces under induced conditions, and enhanced with MMC (gray bars), indicative of the development of a reticular ECM meshwork. (ii) In addition, the average number of spaces during adipogenesis exhibited parallel dynamics seen in Figure 3; with a faster and steeper increase under +MMC conditions. $*p < 0.05$, $**p < 0.01$ and $***p < 0.001$. Color images available online at www.liebertpub.com/tea
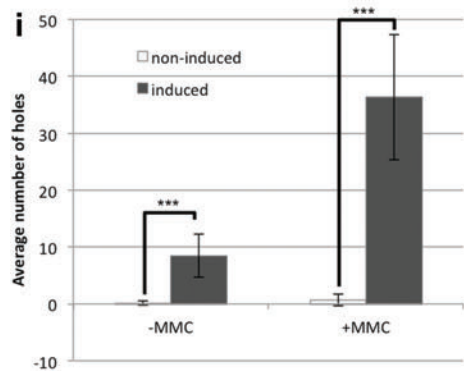
A Col IV directional alignment after 3 weeks of adipogenic differentiation
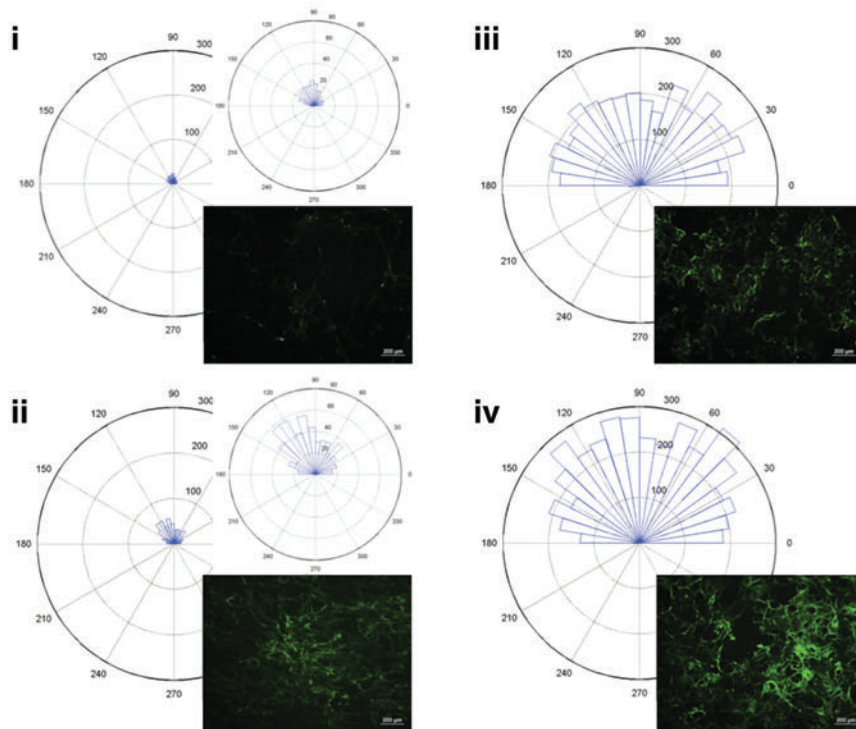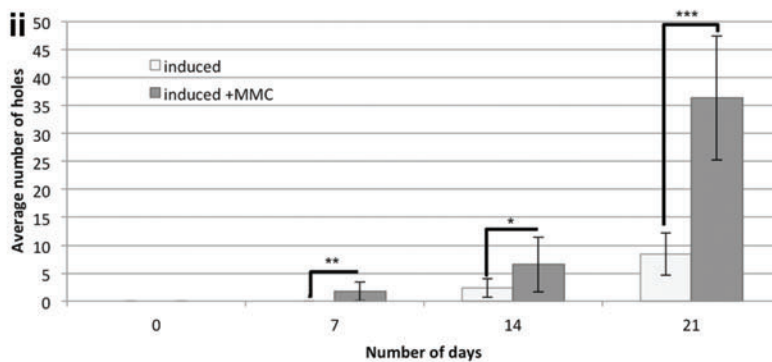
B i Col IV directional alignment during adipogenic differentiation
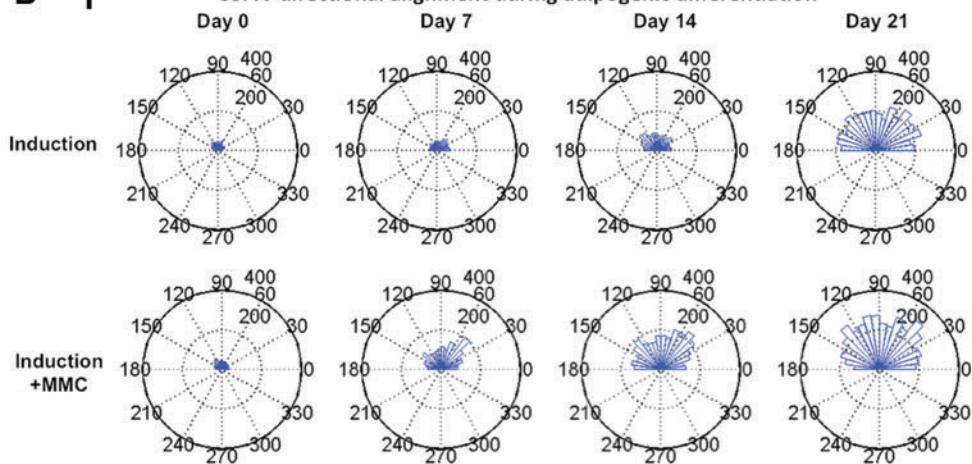
C i Space analysis of Col IV network after 3 weeks of adipogenic differentiation

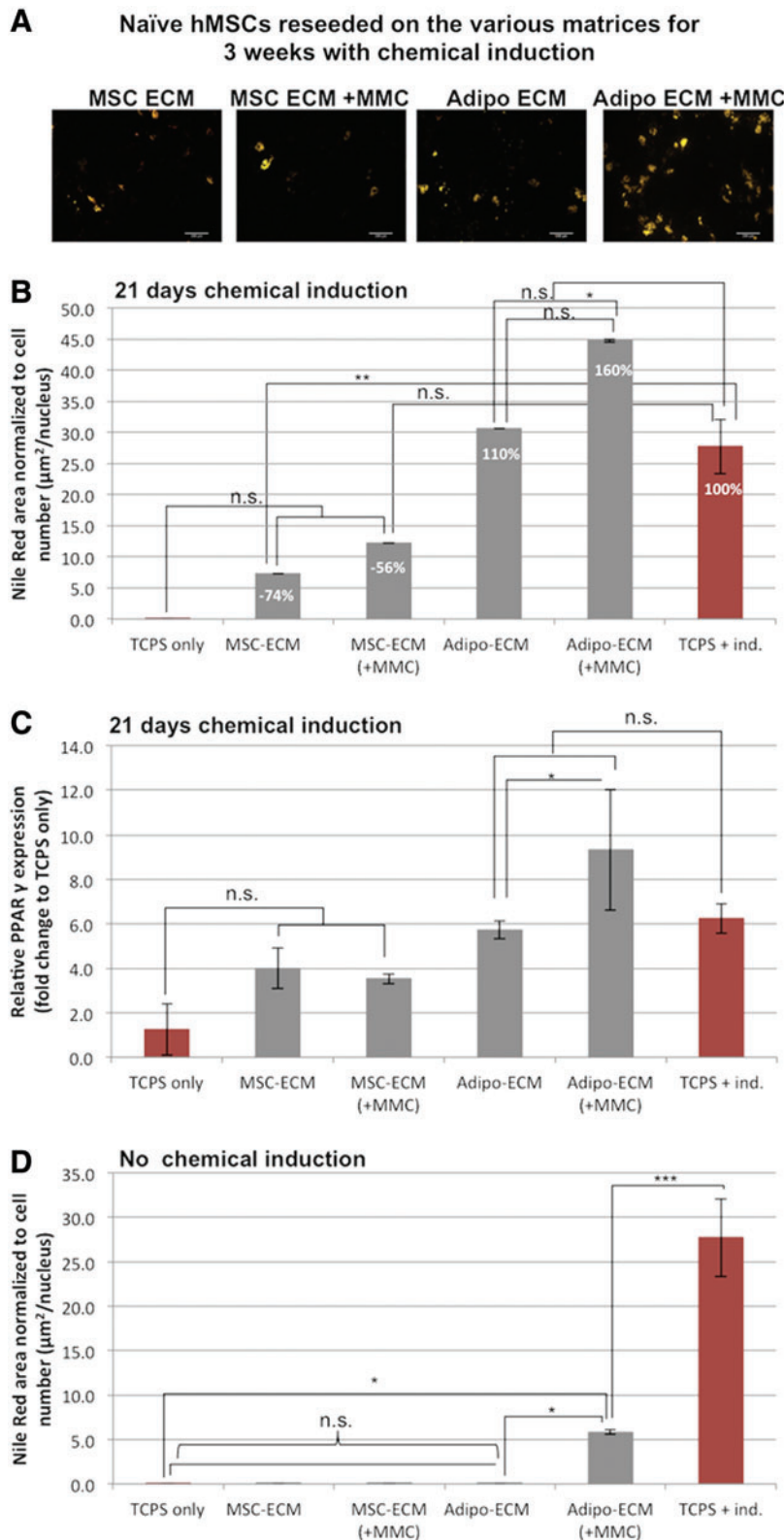Space analysis of Col IV network during adipogenic differentiation

FIG. 7. Adipocyte-derived ECM generated under MMC substantially augments chemically induced adipogenesis. Undifferentiated MSCs were seeded on decellularized ECM generated by undifferentiated MSCs (MSC-ECM) and adipogenically differentiated MSCs (Adipo-ECM) ± MMC and were chemically induced into adipogenesis for 21 days. Lipid droplets were then stained with Nile Red. **(A)** Fluorescent images show most lipid droplet accumulation in cells differentiated on Adipo-ECM (+MMC). Scale bar: 200 μm. **(B)** Quantitation of fluorescent lipid area normalized to cell number demonstrated a 60% increase in lipid droplet accumulation for MSCs differentiated on Adipo-ECM (+MMC) compared with 10% on Adipo-ECM matrices relative to TCPS controls. In contrast, decellularized naïve-state MSC-ECM (±MMC) led to a substantial reduction of lipid droplet accumulation representing 50% of that seen on TCPS controls. **(C)** This was also reflected by relative mRNA expression levels for PPARγ showing a similar increase for MSCs seeded on Adipo-ECM (+MMC). **(D)** Without chemical induction, re-seeded naïve-state MSCs did not exhibit significant lipid droplet accumulation after 21 days except for those seeded on Adipo-ECM (+MMC), which exhibited a five-fold increase in lipid droplet accumulation suggesting spontaneous adipogenic differentiation. $*p < 0.05$, $**p < 0.01$ and $***p < 0.001$. Color images available online at www.liebertpub.com/tea

observed a four-fold increase in Col IV deposition throughout the entire 3-week time course of adipogenic differentiation. Further, we observed a strong and rapid conversion of procollagen I to Col I along with a substantial increase in HSPG deposition in the ECM.

A critical feature of tissue and cellular differentiation is the dynamic remodeling of ECM, encompassing both stoichiometric changes in the total and relative amounts of matrix components within a given tissue volume and cell-mediated re-arrangement of structural features of the ECM.

Here, we provide novel evidence in a human model that both stoichiometric and geometric changes of ECM during adipogenesis of MSCs occur *in-vitro*, and that these changes are intensified under MMC. We have semiquantitative evidence for a shift of Col I toward Col IV content and a reduction of FN content. The most striking evidence for remodeling are the geometric ECM changes that show a transition of linearly/parallelly aligned deposition pattern of ECM components to a characteristic "honey-comb" pattern. This is the first systematic study of ECM changes *in-vitro* during adipogenesis of human MSCs, and its augmentation through MMC. These observations extend those previously made in murine preadipoctyes[25] and graphically demonstrate *in-vitro* how MSCs also remodel their microenvironment geometrically when they change from spindle-shaped cells to the round lipid-laden adipocytes. ECM remodeling MMP activity has been suggested as a key trigger for adipogenic differentiation, by which morphological and cytoskeletal reorganization leads to the induction of mRNA expression of lipogenic proteins.[35] Notably, MMP-2 and MMP-9 secretion is increased during adipocyte differentiation in both human adipocytes and the murine 3T3-F442A cell line.[28] We have now confirmed the presence of MMP-2 in a human MSC cell layer through the course of differentiation

and its marked elevation with MMC. This is in keeping with our recent demonstration that MMC enhances a wide range of enzymatic activities, including DNA polymerase, reverse transcriptase,[36] lysyl oxidase, transglutaminase, and proteases such as BMP-1[15] (Supplementary Fig. S3). Using bacterial collagenase, we demonstrated that MMC, in fact, also accelerates MMP activity. It is, therefore, plausible that the necessary turn-over and change in ECM composition during adipogenesis is enhanced under conditions of MMC by an increased presence and activity of MMPs. This finding adds a novel facet to the various effects that MMC exerts on matrix formation,[15] and it also has a bearing on general considerations in tissue engineering approaches. MMPs are an intrinsic feature of tissues during maintenance, development, or remodeling tissues.[37,38] The ability of MMC to intensify MMP activity *in-vitro* might, therefore, be exploited to study tissue remodeling and MMP inhibitors in models recently described.[39] Our finding might explain recent observations on chondrogenic pellet cultures that appeared less stable under MMC.[40]

The amplified adipogenesis in MSC under crowded conditions suggested a positive feedback from the nascent and transforming ECM to differentiating cells. This phenomenon has been originally described as dynamic cell-matrix

FIG. 8. Schematic representation of adipogenic cell-matrix reciprocity in MSCs as driven by a microenvironment enhanced by MMC. MMC increases ECM deposition by spindle-shaped undifferentiated MSCs, including collagen I, IV, fibronectin, and heparan sulfate proteoglycans (HSPG), here perlecan. Collagen IV, a major component of the basement membrane, is predominant in the matrix of adipose tissue, providing structural support to lipid-laden adipocytes. As differentiation ensues, the geometry and composition of these matrices are remodeled, which is mirrored by a rounded cell morphology. Increased presence of HSPG in the adipocyte matrix suggests increased sequestration of adipogenically relevant growth factors such as fibroblast growth factor-2 (FGF-2), which are secreted by MSC in an autocrine fashion. This results in a positive feedback loop (as shown by the arrows) guiding differentiating MSCs deeper into adipogenic maturation. Color images available online at www.liebertpub.com/tea
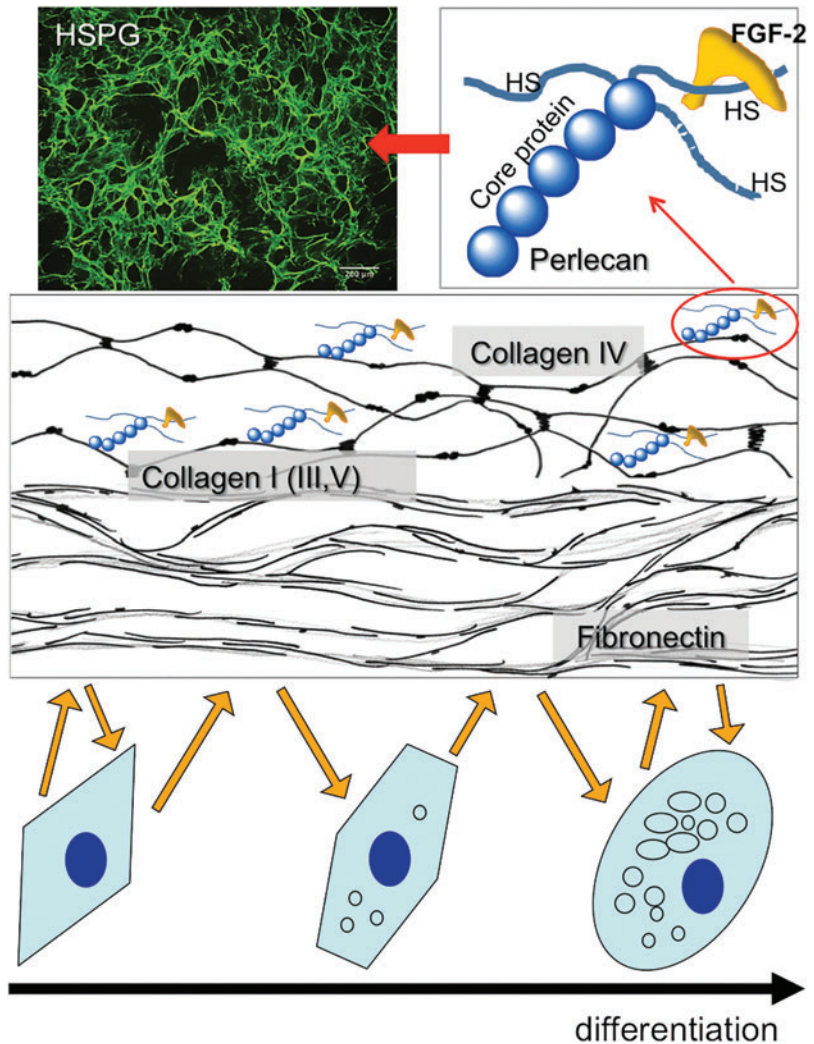
reciprocity in the context of cancer-stroma relationships.[41] We hypothesized that cell-matrix reciprocity is responsible for the increased adipogenesis under MMC and, therefore, investigated the adipogenic potential of decellularized ECM generated by MSCs adipogenically induced in the presence or absence of MMC.

We show here for the first time in a human cell system that the adipogenic lineage-directing information is retained more strongly in matrices which have been laid down by differentiating cells under MMC. After 10 days of chemical induction, MSCs differentiated on MMC-generated Adipo-ECM (Adipo-ECM+MMC) matrices show an accelerated adipogenesis, with lipid droplet accumulation being increased by more than 200-fold compared with TCPS alone and five-fold compared with MSCs seeded on Adipo-matrices generated without MMC. In fact, when MSCs were seeded onto Adipo-ECM+MMC matrices without chemical induction, a five-fold increase in lipid droplet accumulation (over TCPS) was evident, indicating spontaneous adipogenic matrix-induced differentiation. Of note, the matrices used were generated via a stringent detergent-based decellularization protocol that led to losses of ECM amounting to 90% (unpublished data). Considering these losses, the remaining lineage-directing information retained in these matrices is remarkable. Dissecting the nature of the adipogenic cues in these matrices is not easy, as the amount of matrix, geometry, the composition of matrix components, the resulting mechanical properties, and the presentation of biochemical cues represented by bound growth factors are intertwined.

The geometry in the matrices might play a role, as undifferentiated MSCs seeded onto such a matrix will be confronted with a reticular rather than a parallelly aligned fibrillar network that influences cell shape and, hence, enhanced adipogenesis.[42] Notably, in the presence of an overwhelming amount of chemical cues (as present in the adipogenic differentiation cocktail), different matrices exerted dampening or supporting effects. Taking tissue culture polystyrene as a benchmark, MSC-ECM (+MMC) dampened adipogenesis considerably as evidenced by reducing the lipid area by 50%. In stark contrast, Adipo-ECM (+MMC) supported adipogenesis as seen from an increase of lipid area by 60% ($p < 0.05$). The thinness of the ECM layers precluded accurate measurements of stiffness or softness but it is conceivable that under MMC, the abundant matrix deposited might insulate the MSCs from the underlying stiffness of TCPS. In fact, soft substrates aid adipogenic differentiation of MSCs,[43,44] but these results are usually obtained using hydrogels (in this reference, a MeHA hydrogel of 200 μm thickness was used). However, the substantial bandwidth of adipogenic responses showed that a layer of fibrillar matrix produced by a monolayer culture can modulate the function of TCPS significantly.

With regard to the composition of ECM, it is intriguing that HSPG deposition is enhanced (four-fold increase at day 21) under MMC, which is concomitant with adipogenic differentiation. HSPGs play an important role in sequestering a variety of growth factors, including fibroblast growth factor (FGF), transforming growth factor (TGF), bone morphogenic proteins, and hepatic growth factor.[45] The higher HSPG content of matrices generated under MMC, therefore, would suggest a higher content of FGF1 and FGF2 in these matrices. Both factors are important in adipogenesis and as survival factors for MSCs in an autocrine fashion. As in our system, MSCs show evidence of FGF2 synthesis (Supplementary Fig. S7), autocrine sequestration of this growth factor into the pericellular matrix, and feedback to cells as described recently[46] appears likely (Fig. 8).

In summary, we have shown that MMC of culture medium to a degree that human MSCs might encounter in bone marrow enables these cells to build a more robust microenvironment. The ECM generated by differentiating cells under MMC during adipogenic induction is more extensively remodeled toward a pro-adipogenic microenvironment. In turn, the resulting enhanced microenvironment promotes the adipogenic differentiation pathway, demonstrating the role of dynamic cell-matrix reciprocity in stem cell culture and its tunability by MMC. This culture system will enable researchers to build more realistic human models of adipogenic cell differentiation and functionality as a viable alternative to murine cell lines.

Authors' Contribution

X.M.A., M.H.C.L., A.B., and M.R. designed the experiments. X.M.A., M.H.C.L., A.B., C.C., and L.L.S.O. carried out the experiments. X.M.A., M.H.C.L., A.B., C.C., L.L.S.O., A.S., and M.R. contributed to data analysis. X.M.A., M.H.C.L., A.S., and M.R. wrote the article, and all authors provided feedback.

Acknowledgments

Disclosure Statement

No competing financial interests exist.

References

1. Pittenger, M.F., Mackay, A.M., Beck, S.C., Jaiswal, R.K., Douglas, R., Mosca, J.D., *et al.* Multilineage potential of adult human mesenchymal stem cells. Science **284,** 143, 1999.

2. Banfi, A., Muraglia, A., Dozin, B., Mastrogiacomo, M., Cancedda, R., and Quarto, R. Proliferation kinetics and differentiation potential of *ex vivo* expanded human bone marrow stromal cells: implications for their use in cell therapy. Exp Hematol **28,** 707, 2000.

3. Fuchs, E., Tumbar, T., and Guasch, G. Socializing with the neighbors: stem cells and their niche. Cell **116,** 769, 2004.

4. Gregory, C.A., Ylostalo, J., and Prockop, D.J. Adult bone marrow stem/progenitor cells (MSCs) are preconditioned by microenvironmental "niches" in culture: a two-stage hypothesis for regulation of MSC fate. Sci STKE **2005,** pe37, 2005.

5. Moore, K.A., and Lemischka, I.R. Stem cells and their niches. Science **311,** 1880, 2006.

6. Blow, N. Cell culture: building a better matrix. Nat Meth **6,** 619, 2009.

7. Auger, F.A., Berthod, F., Moulin, V., Pouliot, R., and Germain, L. Tissue-engineered skin substitutes: from *in vitro*

constructs to *in vivo* applications. Biotechnol Appl Biochem **39(Pt 3),** 263, 2004.

8. Lareu, R.R., Arsianti, I., Subramhanya, H.K., Yanxian, P., and Raghunath, M. *In vitro* enhancement of collagen matrix formation and crosslinking for applications in tissue engineering: a preliminary study. Tissue Eng **13,** 385, 2007.

9. Lareu, R.R., Subramhanya, K.H., Peng, Y., Benny, P., Chen, C., Wang, Z., *et al.* Collagen matrix deposition is dramatically enhanced *in vitro* when crowded with charged macromolecules: the biological relevance of the excluded volume effect. FEBS Lett **581,** 2709, 2007.

10. Ellis, R.J. Macromolecular crowding: an important but neglected aspect of the intracellular environment. Curr Opin Struct Biol **11,** 114, 2001.

11. Aukland, K., Kramer, G.C., and Renkin, E.M. Protein concentration of lymph and interstitial fluid in the rat tail. Am J Physiol **247(1 Pt 2),** H74, 1984.

12. Bates, D.O., Levick, J.R., and Mortimer, P.S. Change in macromolecular composition of interstitial fluid from swollen arms after breast cancer treatment, and its implications. Clin Sci **85,** 737, 1993.

13. Wadsworth, G.R., and Oliveiro, C.J. Plasma protein concentration of normal adults living in Singapore. Br Med J **2,** 1138, 1953.

14. Madden, T.L., and Herzfeld, J. Crowding-induced organization of cytoskeletal elements: I. Spontaneous demixing of cytosolic proteins and model filaments to form filament bundles. Biophys J **65,** 1147, 1993.

15. Chen, C., Loe, F., Blocki, A., Peng, Y., and Raghunath, M. Applying macromolecular crowding to enhance extracellular matrix deposition and its remodeling *in vitro* for tissue engineering and cell-based therapies. Adv Drug Deliv Rev **63,** 277, 2011.

16. Drenckhahn, D., and Pollard, T.D. Elongation of actin filaments is a diffusion-limited reaction at the barbed end and is accelerated by inert macromolecules. J Biol Chem **261,** 12754, 1986.

17. Minton, A.P. Influence of excluded volume upon macromolecular structure and associations in "crowded" media. Curr Opin Biotechnol **8,** 65, 1997.

18. Chen, C.Z.C., Peng, Y.X., Wang, Z.B., Fish, P.V., Kaar, J.L., Koepsel, R.R., *et al.* The Scar-in-a-Jar: studying potential antifibrotic compounds from the epigenetic to extracellular level in a single well. Br J Pharmacol **158,** 1196, 2009.

19. Zeiger, A.S., Loe, F.C., Li, R., Raghunath, M., and Van Vliet, K.J. Macromolecular crowding directs extracellular matrix organization and mesenchymal stem cell behavior. PLoS One **7,** e37904, 2012.

20. Poulos, S.P., Dodson, M.V., and Hausman, G.J. Cell line models for differentiation: preadipocytes and adipocytes. Exp Biol Med (Maywood) **235,** 1185, 2010.

21. Greenspan, P., Mayer, E.P., and Fowler, S.D. Nile red: a selective fluorescent stain for intracellular lipid droplets. J Cell Biol **100,** 965, 1985.

22. Gimble, J.M., Morgan, C., Kelly, K., Wu, X., Dandapani, V., Wang, C.S., *et al.* Bone morphogenetic proteins inhibit adipocyte differentiation by bone marrow stromal cells. J Cell Biochem **58,** 393, 1995.

23. Yoon, C-H., Hur, J., Park, K-W., Kim, J-H., Lee, C-S., Oh, I-Y., *et al.* Synergistic neovascularization by mixed transplantation of early endothelial progenitor cells and late outgrowth endothelial cells: the role of angiogenic

24. Gregoire, F.M., Smas, C.M., and Sul, H.S. Understanding adipocyte differentiation. Physiol Rev **78,** 783, 1998.

25. Lilla, J., Stickens, D., and Werb, Z. Metalloproteases and adipogenesis: a weighty subject. Am J Pathol **160,** 1551, 2002.

26. Spiegelman, B.M., and Ginty, C.A. Fibronectin modulation of cell shape and lipogenic gene expression in 3T3-adipocytes. Cell **35(3 Pt 2),** 657, 1983.

27. Sillat, T., Saat, R., Pöllänen, R., Hukkanen, M., Takagi, M., and Konttinen, Y.T. Basement membrane collagen type IV expression by human mesenchymal stem cells during adipogenic differentiation. J Cell Mol Med **16,** 1485, 2012.

28. Bouloumié A, Sengenès, C., Portolan, G., Galitzky, J., and Lafontan, M. Adipocyte produces matrix metalloproteinases 2 and 9: involvement in adipose differentiation. Diabetes **50,** 2080, 2001.

29. Cheung, M.S., Klimov, D., and Thirumalai, D. Molecular crowding enhances native state stability and refolding rates of globular proteins. Proc Natl Acad Sci USA **102,** 4753, 2005.

30. Harve, K.S., Lareu, R., Rajagopalan, R., and Raghunath, M. Understanding how the crowded interior of cells stabilizes DNA/DNA and DNA/RNA hybrids-in silico predictions and *in vitro* evidence. Nucleic Acids Res **38,** 172, 2010.

31. Zimmerman, S.B., and Minton, A.P. Macromolecular crowding: biochemical, biophysical, and physiological consequences. Annu Rev Biophys Biomol Struct **22,** 27, 1993.

32. Folkow, B., Gurèvich, M., Hallbäck, M., Lundgren, Y., and Weiss, L. The hemodynamic consequences of regional hypotension in spontaneously hypertensive and normotensive rats. Acta Physiol Scand **83,** 532, 1971.

33. Grisendi, G., Annerén, C., Cafarelli, L., Sternieri, R., Veronesi, E., Cervo, G.L., *et al.* GMP-manufactured density gradient media for optimized mesenchymal stromal/stem cell isolation and expansion. Cytotherapy **12,** 466, 2010.

34. Mariman, E.C.M., and Wang, P. Adipocyte extracellular matrix composition, dynamics and role in obesity. Cell Mol Life Sci **67,** 1277, 2010.

35. Huang, G., and Greenspan, D.S. ECM roles in the function of metabolic tissues. Trends Endocrinol Metab **23,** 16, 2012.

36. Lareu, R.R., Harve, K.S., and Raghunath, M. Emulating a crowded intracellular environment *in vitro* dramatically improves RT-PCR performance. Biochem Biophys Res Commun **363,** 171, 2007.

37. Ravanti, L., and Kähäri, V.M. Matrix metalloproteinases in wound repair (review). Int J Mol Med **6,** 391, 2000.

38. Birkedal-Hansen, H., Moore, W.G., Bodden, M.K., Windsor, L.J., Birkedal-Hansen, B., DeCarlo, A., *et al.* Matrix metalloproteinases: a review. Crit Rev Oral Biol Med **4,** 197, 1993.

39. Neagoș, D., Mitran, V., Chiracu, G., CIUBĂR, R., and IANCU, C. Neagoş: Skin wound healing in a free floating fibroblast... - Google Scholar. Rom J Biophys **16,** 157, 2006.

40. Chen, B., Wang, B., Zhang, W.J., Zhou, G., Cao, Y., and Liu, W. Macromolecular crowding effect on cartilaginous matrix production: a comparison of two-dimensional and three-dimensional models. Tissue Eng Part C Methods **19,** 586, 2013.

41. Bissell, M.J., and Aggeler, J. Dynamic reciprocity: how do extracellular matrix and hormones direct gene expression? Prog Clin Biol Res **249,** 251, 1987.

42. McBeath, R., Pirone, D.M., Nelson, C.M., Bhadriraju, K., and Chen, C.S. Cell shape, cytoskeletal tension, and RhoA

regulate stem cell lineage commitment. Dev Cell **6,** 483, 2004.

43. Park, J.S., Chu, J.S., Tsou, A.D., Diop, R., Tang, Z., Wang, A., *et al.* The effect of matrix stiffness on the differentiation of mesenchymal stem cells in response to TGF-β. Biomaterials **32,** 3921, 2011.

44. Guvendiren, M., and Burdick, J.A. Stiffening hydrogels to probe short-and long-term cellular responses to dynamic mechanics. Nat Commun **3,** 792, 2012.

45. Taipale, J., and Keski-Oja, J. Growth factors in the extracellular matrix. FASEB J **11,** 51, 1997.

46. Kim, J., and Ma, T. Autocrine fibroblast growth factor 2-mediated interactions between human mesenchymal stem cells and the extracellular matrix under varying oxygen tension. J Cell Biochem **114,** 716, 2013.

Address correspondence to:
Michael Raghunath, MD, PhD
Department of Biomedical Engineering
Faculty of Engineering
National University of Singapore
9 Engineering Drive 1
Block EA #03-12
Singapore 117575
Singapore

E-mail: bierm@nus.edu.sg